Water Splitting

DOI: 10.1002/ange.201408374

Enhanced Water Splitting at Thin Film Tungsten Trioxide Photoanodes Bearing Plasmonic Gold–Polyoxometalate Particles**

Renata Solarska, Krzysztof Bienkowski, Sylwia Zoladek, Aldona Majcher, Tomasz Stefaniuk, Pawel J. Kulesza, and Jan Augustynski*

Abstract: *Tungsten trioxide (WO_3) is one of a few stable semiconductor materials liable to produce solar fuel by photoelectrochemical water splitting. To enhance its visible light conversion efficiency, we incorporated plasmonic gold nanoparticles (Au NPs) derivatized with polyoxometalate ($H_3PMo_{12}O_{40}$) species into WO_3. The combined plasmonic and catalytic effect of Au NPs anchored to the WO_3 surface resulted in a large increase of water photooxidation currents. Shielding the Au NPs with polyoxometalates appears to be an effective means to avoid formation of recombination centers at the photoanode surface.*

Since several decades, efficient water splitting in photoelectrochemical cells is a target of continuing research.[1] Significant progress has recently been made in the development of n-type metal oxide semiconductors that are able to act as sunlight-driven photoanodes for oxygen formation. Whereas many of the ongoing efforts focus on decreasing the additional electrical bias required to photooxidize water, another important issue for the semiconducting oxides, characterized by indirect optical transition, are the long absorption depths in the visible range of the solar spectrum.

This is in particular the case for tungsten trioxide (WO_3), which exhibits a low absorption coefficient near the fundamental band edge that increases quite slowly at shorter wavelengths. In WO_3, which in its monoclinic form has a band gap energy of 2.5 eV, the long optical pathways correspond to visible wavelengths (400–500 nm), that determine the quantity of solar radiation absorbed by the photoanode material.[2a] This issue is also critical for semiconductors which suffer from particularly short diffusion length of minority and/or majority charge carriers and for which the light absorption extends far away from the space–charge layer. In such cases, given that the light absorption occurring in part at a large distance from the semiconductor–electrolyte interface, the incorporation into the semiconductor of plasmonic metal nanoparticles (NPs) provides a means to localize photon absorption close to the surface. In thin-film photovoltaic cells, enhanced light trapping has already been demonstrated through scattering by plasmonic gold or silver NPs incorporated within the cell.[3] For example, a photocurrent increase of up to 16-fold at long wavelengths and an over 30% integrated increase across the solar spectrum have been reported for a thin-film silicon photovoltaic cell.[3b] A remarkable increase in the solar energy conversion efficiency has also been reported for organic heterojunction solar cells that employ a thin plasmon-active layer.[3a,c,d] Intense research in this field has focused not only on the optical and electronic properties of the metal NPs but also on light-management architectures to optimize the efficiency for a particular device.[4]

Whereas the improved light trapping in the photovoltaic cells takes mainly advantage from scattering by plasmonic metal particles,[3b] the light absorption in the metal NPs plays an important role in photoelectrochemical water splitting.[5] The localized surface plasmon resonance, which arises from the oscillations of free electrons in metal particles upon excitation with the resonant photons, induces evanescent optical waves that are trapped near the surface of the semiconductor.[6] The existence of a resonant coupling between the metal NPs and the semiconductor (where the photon absorption spectra of the metal NP and the semiconductor overlap) enables the transfer of the excitation energy from the metal NP to the adjacent semiconductor.[7] Such a surface-plasmon-induced local electromagnetic field effect results in an enhanced formation of the electron–hole pairs in the semiconductor and, possibly, in an increased reaction photocurrent. In addition to the localized light absorption close to the semiconductor surface, the plasmonic metal NPs can further enhance absorbance of the semiconductor film by scattering the incident light, the latter effect becoming dominant for larger particles (at a size of ca. 100 nm for gold particles).[8] Consequently, a thinner semiconductor layer can be used to achieve absorption of the major part of the band-gap photon wavelengths. Moreover, the light scattering by metal NPs placed at the semiconductor surface can also decrease the light reflection that results from the high refractive index of typical semiconductors.[4a,5b] We previously demonstrated the application for water splitting of plasmon-

[*] Dr. R. Solarska, Dr. S. Zoladek, A. Majcher, Prof. P. J. Kulesza
Faculty of Chemistry, University of Warsaw
Pasteura 1, 02-093 Warsaw (Poland)
E-mail: rsolarska@chem.uw.edu.pl
Dr. T. Stefaniuk
Faculty of Physics, University of Warsaw
Pasteura 7, 02-093 Warsaw (Poland)
K. Bienkowski, Prof. J. Augustynski
Centre of New Technologies, University of Warsaw
Banacha 2c, 02-097 Warsaw (Poland)

[**] Financial support from the Maestro Project 2012/04A/ST4/00287 to P. J. Kulesza, awarded by the National Science Center (Poland), is acknowledged. This work was also supported by the OPUS Grant 2011/03/B/ST5/02746 (National Science Centre) to J. Augustynski. This project has received funding from the European Union Seventh Framework Programme (FP7/2007-2013) under grant agreement no. NMP4-SL-2012-3100333.

Supporting information for this article is available on the WWW under http://dx.doi.org/10.1002/anie.201408374.

active silver nanostructures embedded within a thin WO_3 film. This photoanode, consisting of a mesoporous WO_3 layer deposited onto a network of sputtered silver NPs demonstrated significant improvement in the photoinduced oxygen generation due to the combined local electromagnetic field effect and light scattering that stem from plasmonic excitation of the Ag NPs.[9]

Here we explored the ability of gold NPs capped with Keggin-type phosphododecamolybdate ($PMo_{12}O_{40}^{3-}$) anions for enhancing sunlight-induced water splitting at thin film WO_3 photoanodes. The deposition of metal NPs onto a semiconducting surface imposes constraints related on one side to the presence of an electrolyte, which may be corrosive, and on the other side, to the possible creation of surface states that act as recombination centers.[7a] To limit quenching processes such as Förster energy transfer in photoelectrochemical devices, thin insulating layers, for example, polymer[10] and SiO_2,[11] were previously intercalated between the plasmonic metal particles and the semiconductor.

As an alternative to such buffer layers, capping agents may be used that are widely applied to stabilize Au NPs.[12] Like the organic capping ligands, such as alkanothiolates or citrates, inorganic polyoxometalates (POMs) can irreversibly adsorb onto, stabilize, activate, or derivatize metal NPs.[13–15] Moreover, the Keggin-type POMs, such as $PMo_{12}O_{40}^{3-}$, exhibit good proton conductivity and can undergo reversible, stepwise multielectron transfer reactions.[14]

Here, we fabricated $PMo_{12}O_{40}^{3-}$-modified gold NPs of uniform sizes ranging from 30 to 40 nm as shown in Figure 1. The $PMo_{12}O_{40}^{3-}$ anions form a film on the Au NPs that is ca. 1–2 nm thick. Due to the electrostatic and stereochemical repulsive interactions between the negatively charged polyoxomolybdate layers, this film may prevent to a large extent the agglomeration of the capped Au NPs. Since the $PMo_{12}O_{40}^{3-}$ anions interact with the gold through the corner oxygen atoms, they occupy a limited number of active catalytic sites on the NPs surfaces. This description is consistent with TEM observations (Figure 1B) which show the arrangement of the polyoxomolybdate-capped Au NPs around the larger WO_3 particles. The $PMo_{12}O_{40}^{3-}$-protected Au NPs are separated one from each other and from the semiconductor particles with no evidence of aggregation. The coverage of the Au NP surface by a self-assembled monolayer of polyoxomolybdate anions is seen as a space separating the Au NPs. It is to be noted that no separating space appears between WO_3 particles subjected to sintering during the high temperature annealing.

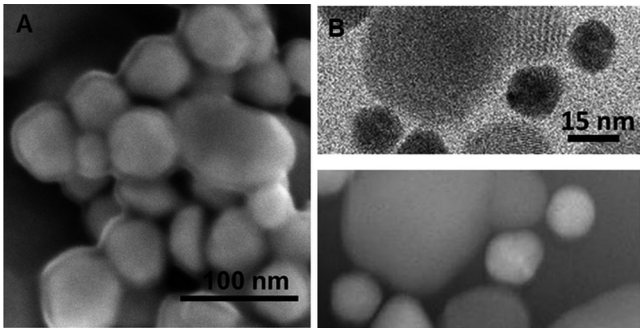

Figure 1. A) SEM and B) TEM images of colloidal gold nanoparticles capped with phosphododecamolybdate adsorbates spread onto a conductive glass substrate (A) and onto a WO_3 film surface (B), and posttreated at 70°C.

X-ray photoelectron spectra (XPS) taken for a sample similar to that of Figure 1B showed the presence of Mo^{VI} and metallic Au signals corresponding to a ca. 3:1 Mo/Au ratio (Figure S1 in the Supporting Information, SI).

For water photooxidation studies, the WO_3 films with Au NPs incorporated in two different configurations were used as photoanodes. In the first case, a mesoporous WO_3 film of ca. 1 μm thickness formed on conductive glass (F-SnO_2, FTO) substrate was decorated with a spread layer of $PMo_{12}O_{40}^{3-}$-capped Au NPs, anchored by a short ($\approx$10 min) annealing at 70°C. In the second configuration, the Au NPs were first deposited on the FTO substrate and became embedded in the subsequently deposited WO_3 film. Given high temperature ($\approx$500°C) annealing involved in the formation of the WO_3 film, a partial aggregation of initially spherical Au NPs in larger particles of irregular shapes, favored by the diffusion and a possible decomposition of $PMo_{12}O_{40}^{3-}$ anions, is expected (see Figure S2A in SI). This kind of gold nanostructure, located at the bottom of the WO_3 film, may act as a reflector and light scatterer during illumination of the photoanode from the solution side. The current–voltage (J–V) water oxidation dependence of a series of WO_3 photoanodes, recorded under simulated solar AM1.5 illumination, is shown in Figure 2. Two main features differentiate J–V profiles recorded for the photoanode with surface anchored Au–$PMo_{12}O_{40}^{3-}$ nanoparticles from the bare WO_3 film.

The onset potential of the water oxidation photocurrent at ca. −0.27 V versus a mercury sulfate electrode (MSE) [corresponding to 0.4 V versus the reversible hydrogen electrode (RHE)] is less positive by ca. 50 mV and, most importantly, the photocurrent plateau is approximately twice

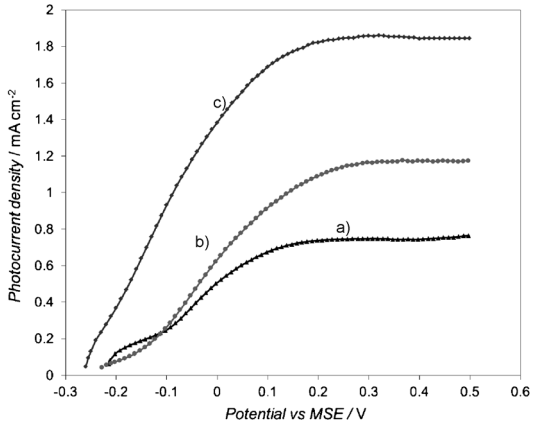

Figure 2. Plots of the photocurrent as a function of the voltage for WO_3 electrodes modified with colloidal gold NPs (b,c) compared with a plot for the bare WO_3 photoanode (a). Curve (b) represents a WO_3 electrode deposited onto Au NPs, curve (c) corresponds to the electrode decorated with the Au NPs. All measurements were performed under simulated AM1.5 sunlight irradiation in a 1 M H_2SO_4 electrolyte.

as large as for the bare WO_3 photoanode. Although these differences are, in part, attributable to the catalytic effect of the polyoxomolybdate-capped Au NPs, another important contribution is the result of plasmonic excitation of the Au NPs. In fact, the Au–$PMo_{12}O_{40}^{3-}$ NPs anchored to the WO_3 surface exhibited plasmonic behavior consistent with the increased visible light absorbance. Comparison of the UV/Vis spectra collected for the Au NPs/WO_3 sample with that of the bare WO_3 film, represented in Figure 3 A, shows a considerably increased absorbance in the range of blue wavelengths

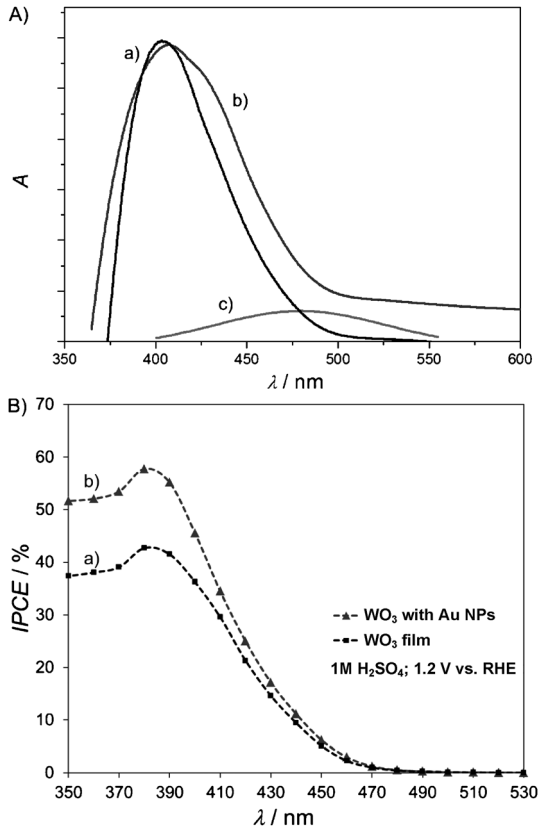

Figure 3. A) Absorbance spectra of a bare WO_3 film of ca. 1 μm thickness (a), and the film decorated with Au NPs (b). Curve (c) represents the spectrum of Au NPs deconvoluted from the experimental curve (b) with $R^2 = 0.9914$. B) IPCE plots for a bare WO_3 photoanode (a) and a WO_3 photoanode decorated with Au NPs (b).

above 420 nm. The absorbance plot for the Au NPs on the WO_3 surface, extrapolated after subtracting the contribution of the WO_3 film, exhibits a maximum at ca. 490 nm, attributable to surface plasmon resonance, with a short wavelengths tail extending to 400 nm. This maximum is slightly blue-shifted with respect to the plasmon band maximum of 520 nm reported for Au NPs of ca. 20 nm in diameter suspended in water.[16] This shift is attributable to the particular dielectric environment of Au NPs including, in the present case, both polyoxomolybdate anions and WO_3. It is also important to mention in this connection that for Au NPs the frequency of interband transitions overlaps with the localized surface plasmon resonance down to ca. 400 nm.[7a,17] This leaves the whole fraction of visible blue wavelengths for the spectral overlap between the surface plasmon resonance of Au NPs and the absorbance of the WO_3 film.

In comparison with the optical absorbance spectra, the incident photon-to-current efficiency (IPCE) spectra of a mesoporous WO_3 photoanode of ca. 1 μm thickness decorated with Au NPs shown in Figure 3 B exhibit a less pronounced increase of the measured photocurrents with respect to the bare WO_3 film. This is especially apparent in the region of lower photon energies close to the band edge.

The observed trend can be understood considering that essentially the whole porous WO_3 film is permeated by the electrolyte and contributes to some extent to the photocurrent. As a consequence of the narrow bandwidth (4 nm) and low intensity of light passing through the monochromator, the generated photocurrents are too weak to allow filling of the electron traps, present within mesoporous WO_3 film, which continue to act as recombination centers. Interestingly, the IPCE spectrum recorded for a thinner, ca. 0.4 μm thick WO_3 photoanode bearing the Au NPs (Figure S3, SI) showed a consistent large increase in the photocurrents versus the film without gold, extending over the whole photoaction spectrum. The observed change in the behavior is to be related to the fact that in this case a larger slab of the photoactive film is located close to the plasmonic Au NPs, within the range of local electromagnetic field interactions.

The differences in the anodic photocurrents represented in Figure 2 were corroborated by the measurements of oxygen production, performed using an oxygen membrane polarographic detector (Figure S4, SI). The levels of oxygen formed at the photoanode decorated with Au–$PMo_{12}O_{40}^{3-}$ NPs, monitored over 1 hour of continuous photoelectrolysis under the AM 1.5 irradiation, were consistently much larger than those at the bare WO_3 photoanode.

To further assess the ability of the colloidal Au NPs used in our photoelectrochemical experiments to generate localized surface plasmons under irradiation with visible light, we performed measurements using scanning near-field optical microscopy (SNOM). In a SNOM experiment, the interaction between the light transferred by a microscope probe terminated with a subwavelength-sized aperture and the plasmonic metal NPs leads to the formation of highly confined electric fields that enhance the transmission. The SNOM sensitivity largely depends on the size, shape, and electric field skin depth of a metal particle. It is to be noted that the spatial resolution of SNOM is superior to that of any other optical imaging method.[18]

The SNOM operational modes employed in our investigations included the transmission and inverted transmission modes, both of which involve an aperture with a diameter of less than 100 nm that is scanned along the sample surface at a distance of approximately 10 nm. Control over the probe–sample distance depends on the detection of the shear forces between the end of the probe and the sample. The SNOM technique allows the simultaneous measurement of a sample's topography and its optical transmission or reflection in the near field. During a scan, the sample is illuminated with laser light that is coupled into the fiber and then transferred to the tapered probe. The light that passed through the sample is then directed through an objective to a photomultiplier tube

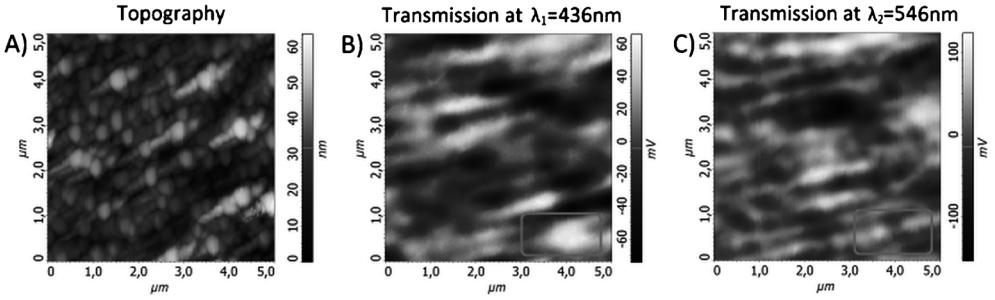

Figure 4. A) SNOM topographic image of the F-SnO_2 substrate spread with colloidal Au NPs. B,C) Parallel images from the photomultiplier recorded at two different wavelengths.

(PMT).[19] The colloidal Au–$PMo_{12}O_{40}^{3-}$ NPs were deposited on the conductive glass FTO support and then the samples were irradiated at two different wavelengths: $\lambda_1 = 436$ nm and $\lambda_2 = 546$ nm. The transmission of light was clearly enhanced by the gold NPs because the SNOM topography, which shows only the large tin oxide crystals of the FTO substrate, differs completely from the images recorded with the PMT as shown in Figure 4. One should also note that the pictures recorded by the PMT under illumination at the two different wavelengths are essentially identical, with the intensity of the illuminated spots varying with the extinction maxima λ_{max} of the particular Au NPs. The SNOM measurements clearly confirmed the occurrence of the plasmonic resonance of the $PMo_{12}O_{40}^{3-}$-capped Au NPs over the range of blue wavelengths overlapping with the absorbance spectrum of WO_3.

On the basis of the presented results it is difficult to precisely assess the relative contribution to the observed enhanced water splitting of the purely catalytic effect of the Au–$PMo_{12}O_{40}^{3-}$ NPs and of the local surface plasmon resonance induced effects. Deposition of $H_3PMo_{12}O_{40}$ alone on the WO_3 surface caused a moderate (by ca. 20%) increase of photooxidation currents (see Figure S5, SI) observed both in H_2SO_4 and CH_3SO_3H electrolytes. At the same time, measurements performed in the latter electrolyte confirmed the large (about 80%) increase of water splitting photocurrents for an WO_3 electrode with anchored Au–$PMo_{12}O_{40}^{3-}$ NPs (Figure S6, SI). The electrocatalytic activity of phosphododecamolybdates that exhibit rapid reversible redox transformations (hopping) between the mixed-valence sites of $Mo^{VI,V}$, is well documented in the literature.[13,14,20] Apparently, they also play a mediating role in the process of water photooxidation and/or by facilitating separation of photogenerated charges. On the other hand, revealed in SNOM measurements, the plasmonic resonance of Au–$PMo_{12}O_{40}^{3-}$ NPs occurring in the region of blue wavelengths overlapping with the absorption spectrum of WO_3, points at the contribution of a local electromagnetic field effect to the observed large enhancement of water splitting photocurrent. It is important to note in this regard that, in contrast with some examples from the literature,[7a] in the present case the incorporation of Au NPs on the WO_3 surface does not lead to the formation of surface states promoting recombination of photogenerated charge carriers. This can be assigned to the shielding effect of the $PMo_{12}O_{40}^{3-}$ anions, which at the acidic pH of the electrolytes used in our photoelectrochemical experiments, are maintained close to the positively charged WO_3-solution interface by electrostatic interactions.

Experimental Section

Synthesis: A suspension of stabilized gold nanoparticles modified with phosphododecamolybdates was prepared by adding the gold precursor $HAuCl_4{\cdot}x\,H_2O$ (puriss. p.a., ACS reagent, $\geq 49\%$ Au basis, Sigma–Aldrich) to a freshly prepared solution of sodium borohydride ($NaBH_4$) and phosphododecamolybdic heteropolyacid ($H_3PMo_{12}O_{40}$). The Keggin-type polyoxometalate acted as the reducing and capping agent. The dispersion and particle size were controlled using the solution temperature and the concentration of the reducing agent. The detailed procedure for preparing and stabilizing the Au NPs has been described earlier.[21]

Electrode preparation: WO_3 films of about 1 µm thickness were prepared using a sol–gel method based on a tungstic acid/poly(ethylene glycol) (PEG) 300 precursor following a previously described procedure.[22] The WO_3 films were formed during three consecutive applications of the precursor followed by annealing in oxygen atmosphere at 500°C for 30 min. Conductive glass FTO plates (Solaronix TCO10-10, 10 $\Omega\,sq^{-1}$) were used as the substrates. The Au NPs were incorporated into the electrode structure either as a monolayer on the FTO substrate or as a WO_3 surface decoration.

Characterization: Scanning electron microscopy (SEM) imaging was performed using a Carl Zeiss AURIGA CrossBeam workstation. The microscope was equipped with "in lens" SE and ExB detectors and a bright-field STEM detector. Transmission electron microscopy (TEM) measurements were carried out using a STEM Hitachi HD2700 microscope equipped with a Schottky field emission electron source and a Cs corrector from CEOS, operating at 200 kV. The photocurrent–voltage plots of the WO_3-based photoanodes were recorded in a 1M H_2SO_4 or a 1M CH_3SO_3H solution under AM1.5 irradiation (100 $mW\,cm^{-2}$) provided by an Oriel 150 Watt solar simulator fitted with a Schott 113 filter and a neutral density filter. The photoanodes were polarized at 10 $mV\,s^{-1}$ using a CHI660 electrochemical workstation; the incident photon-to-current conversion efficiencies (IPCEs), as a function of the excitation wavelength, were determined by illuminating the sample with the light from a 500 Watt xenon lamp through a Multispec 257 monochromator (Oriel) with a bandwidth of 4 nm. Optical absorption spectra were acquired using a Jasco V-600 spectrophotometer equipped with a 16 mm integrating sphere. The SNOM allowed the simultaneous measurement of the sample topography and of the optical transmission (reflection) of the sample in the near-field. In the transmission mode, the laser light was coupled with the fiber and transferred to the tapered probe, which acted as a subwavelength light source. Then, the light passing through the sample was collected by the objective and was directed into the photomultiplier tube (PMT).

Received: August 20, 2014
Published online: October 21, 2014

Keywords: Keggin-type structures · plasmonic gold nanoparticles · polyoxometalates · solar energy conversion · tungsten trioxide

[1] a) F. E. Osterloh, *Chem. Soc. Rev.* **2013**, *42*, 2294 – 2320; b) A. Valdés, J. Brillet, M. Graetzel, H. Gudmundsdottir, H. A. Hansen, H. Jonsson, P. Klupfel, G. J. Kroes, F. Le Formal, I. C. Man, R. S. Martins, J. K. Norskov, J. Rossmeisl, K. Sivula, A. Vojvodic, M. Zach, *Phys. Chem. Chem. Phys.* **2012**, *14*, 49 – 70; c) X. Liu, F. Wang, Q. Wang, *Phys. Chem. Chem. Phys.* **2012**, *14*, 7894 – 7911.

[2] a) J. Augustyński, B. D. Alexander, R. Solarska, *Topics in Current Chemistry, Vol. 303* (Ed.: C. A. Bignozzi), Springer, Berlin, **2011**, pp. 1 – 38; b) T. Woo Kim, K.-S. Choi, *Science* **2014**, *343*, 990 – 994.

[3] a) T. H. Reilly, J. van de Lagemaat, R. C. Tenent, A. J. Morfa, K. L. Rowlen, *Appl. Phys. Lett.* **2008**, *92*, 243304; b) S. Pillai, K. R. Catchpole, T. Trupke, M. A. Green, *J. Appl. Phys.* **2007**, *101*, 093105; c) A. J. Morfa, K. L. Rowlen, T. H. Reilly, M. J. Romero, J. van de Lagemaat, *Appl. Phys. Lett.* **2008**, *92*, 013504; d) S. S. Kim, S. I. Na, J. Jo, D. Y. Kim, Y. Ch. Nah, *Appl. Phys. Lett.* **2008**, *93*, 073307.

[4] a) H. A. Atwater, A. Polman, *Nat. Mater.* **2010**, *9*, 205 – 213; b) A. Polman, H. A. Atwater, *Nat. Mater.* **2012**, *11*, 174 – 177.

[5] a) S. Linic, P. Christopher, D. B. Ingram, *Nat. Mater.* **2011**, *10*, 911 – 921; b) S. C. Warren, E. Thimsen, *Energy Environ. Sci.* **2012**, *5*, 5133 – 5146; c) W. Hou, S. B. Cronin, *Adv. Funct. Mater.* **2013**, *23*, 1612 – 1619.

[6] W. L. Barnes, A. Dereux, T. W. Ebbesen, *Nature* **2003**, *424*, 824 – 830.

[7] a) E. Thimsen, F. Le Formal, M. Gratzel, S. C. Warren, *Nano Lett.* **2011**, *11*, 35 – 43; b) J. T. Li, S. K. Cushing, J. Bright, F. K. Meng, T. R. Senty, P. Zheng, A. D. Bristow, N. Q. Wu, *Acs Catal.* **2013**, *3*, 47 – 51.

[8] A. Tcherniak, J. W. Ha, S. Dominguez-Medina, L. S. Slaughter, S. Link, *Nano Lett.* **2010**, *10*, 1398 – 1404.

[9] a) R. Solarska, A. Krolikowska, J. Augustynski, *Angew. Chem. Int. Ed.* **2010**, *49*, 7980 – 7983; *Angew. Chem.* **2010**, *122*, 8152 – 8155; b) R. Solarska, A. Krolikowska, K. Bienkowski, T. Stefaniuk, J. Augustynski, *Energy Procedia* **2012**, *22*, 137 – 146.

[10] D. B. Ingram, S. Linic, *J. Am. Chem. Soc.* **2011**, *133*, 5202 – 5205.

[11] S. K. Cushing, J. Li, F. Meng, T. R. Senty, S. Suri, M. Zhi, M. Li, A. D. Bristow, N. Wu, *J. Am. Chem. Soc.* **2012**, *134*, 15033 – 15041.

[12] a) R. Sardar, A. M. Funston, P. Mulvaney, R. W. Murray, *Langmuir* **2009**, *25*, 13840 – 13851; b) M. Lublow, K. Skorupska, S. Zoladek, P. J. Kulesza, T. Vo-Dinh, H. J. Lewerenz, *Electrochem. Commun.* **2010**, *12*, 1298 – 1301.

[13] A. Sartorel, M. Bronchio, S. Campagna, F. Scandola, *Chem. Soc. Rev.* **2013**, *42*, 2262 – 2280.

[14] a) J. B. Moffat, *Metal-oxygen clusters: the surface and catalytic properties of heteropoly oxometalates*, Kluwer Academic/Plenum Publisher, New York, **2001**; b) M. Vazylyev, D. Sloboda-Rozner, A. Haimov, G. Maayan, R. Neumann, *Top. Catal.* **2005**, *34*, 93 – 99.

[15] A. Troupis, A. Hiskia, E. Papaconstantinou, *Angew. Chem. Int. Ed.* **2002**, *41*, 1911 – 1914; *Angew. Chem.* **2002**, *114*, 1991 – 1994.

[16] S. Link, M. A. El-Sayed, *J. Phys. Chem. B* **1999**, *103*, 4212 – 4217.

[17] M. V. Uwe Kreibig, *Optical Properties of Metal Clusters, Vol. 25*, Springer, Heidelberg, **1995**.

[18] C. Genet, T. W. Ebbesen, *Nature* **2007**, *445*, 39 – 46.

[19] E. Betzig, P. L. Finn, J. S. Weiner, *Appl. Phys. Lett.* **1992**, *60*, 2484 – 2486.

[20] D. Martel, A. Kuhn, *Electrochim. Acta* **2000**, *45*, 1829 – 1836.

[21] A. Z. Ernst, S. Zoladek, K. Wiaderek, J. A. Cox, A. Kolary-Zurowska, K. Miecznikowski, P. J. Kulesza, *Electrochim. Acta* **2008**, *53*, 3924 – 3931.

[22] C. Santato, M. Odziemkowski, M. Ulmann, J. Augustynski, *J. Am. Chem. Soc.* **2001**, *123*, 10639 – 10649.